EPJ Photovoltaics **13**, 28 (2022)

https://doi.org/10.1051/epjpv/2022026

Available online at:
www.epj-pv.org

Special Issue on 'WCPEC-8: State of the Art and Developments in Photovoltaics', edited by Alessandra Scognamiglio, Robert Kenny, Shuzi Hayase and Arno Smets

REGULAR ARTICLE OPEN ACCESS

Impact of Ag content on device properties of Cu(In,Ga)Se_2 solar cells

Ana Kanevce[1,*], Stephanie Essig[2], Stefan Paetel[1], Wolfram Hempel[1], Dimitrios Hariskos[1], and Theresa Magorian Friedlmeier[1]

[1] Zentrum für Sonnenenergie und Wasserstoff Forschung, 70563 Stuttgart, Germany
[2] Institute for Photovoltaics, University of Stuttgart, 70569 Stuttgart, Germany

Received: 30 June 2022 / Received in final form: 13 October 2022 / Accepted: 15 November 2022

Abstract. Partial substitution of Cu by Ag in Cu(In,Ga)Se_2 (CIGS) solar cells is advantageous as it allows lower temperature growth while maintaining high performance. To understand the role of Ag on device performance, we present a comprehensive analysis of (Ag,Cu)(In,Ga)Se_2 (ACIGS) samples with an [Ag]/([Ag]+[Cu]) (AAC) ratio varying from 7% to 22%. The analysis involves a set of material and device characterization techniques as well as numerical simulations. Multiple electrical and material properties show a systematic dependence on the increased Ag content. These include a carrier-density decrease, a grain-size increase, and a flattened [Ga]/([Ga] + [In]) (GGI) profile leading to a higher minimum band gap energy and a reduced back grading. Although the best performing device (PCE = 18.0%) in this set has an AAC = 7%, cells with higher Ag contents have an advantage of a smoother absorber surface which is attractive for tandem applications, despite their slightly inferior conversion efficiencies (PCE = 16.4% for 22% Ag).

Keywords: Ag / CIGS solar cells / material characterization / device characterization

1 Introduction

Despite the higher price of Ag in comparison to Cu, a partial substitution of Cu with Ag in Cu(In,Ga)Se_2 solar cells can be attractive from an industrial perspective, as it allows a lower growth temperature without a significant performance loss. In addition, Ag-containing CIGS is shown to have a smoother surface [1,2], beneficial for tandem solar cells.

In this work, we aim to improve the understanding of the role of silver incorporation in CIGS cells. Therefore, a sample series with five different AAC ratios from 7% to 22% was subjected to a characterization analysis containing multiple material and device characterization techniques: current-voltage as a function of temperature and illumination intensity, quantum efficiency (QE), capacitance-voltage (CV), scanning electron microscopy (SEM), glow discharge optical emission spectroscopy (GDOES) and time-of-flight secondary ion mass spectroscopy (ToF-SIMS).

The (Ag,Cu)(In,Ga)Se_2 absorbers were grown by co-evaporation in an inline deposition chamber at a maximum substrate heater temperature of 580°C on a Mo-coated soda-lime glass substrate. More details about the ACIGS and the deposition process can be found in references [2,3]. The solar-cell stack consists of a ~2-μm-thick ACIGS absorber, a 50-nm-thick CdS buffer layer deposited by chemical bath deposition, a sputtered 80-nm i-ZnO, and a 230-nm Al-ZnO layer. The absorbers received a RbF post-deposition treatment.

The current–voltage measurements were performed at a temperature of 25 °C under AM1.5 illumination. The intensity-dependent current voltage curves were measured using neutral density filters. The temperature-dependent JV measurements were performed from 300 K to 130 K in a liquid-nitrogen cooled cryostat with a Xe-lamp illumination. External quantum efficiency measurements were performed with a chopped monochromatic light under white light bias from a QH lamp and at zero voltage bias. The reflection measurements used to determine the internal quantum efficiency (IQE) were performed with an integrated sphere. The capacitance-voltage sweeps were performed at room temperature scanned from negative to positive voltage values. Scanning electron microscopy (SEM) images were generated in a Zeiss Crossbeam 550. Compositional depth profiling was performed by glow discharge optical emission spectroscopy (GDOES). ToF-SIMS Depth-profiles were run with Bi-ion-gun as an analyzing source and O_2-ion-gun as a sputtering source, to maintain a good sensibility for alkaline elements.

* e-mail: ana.kanevce@zsw-bw.de

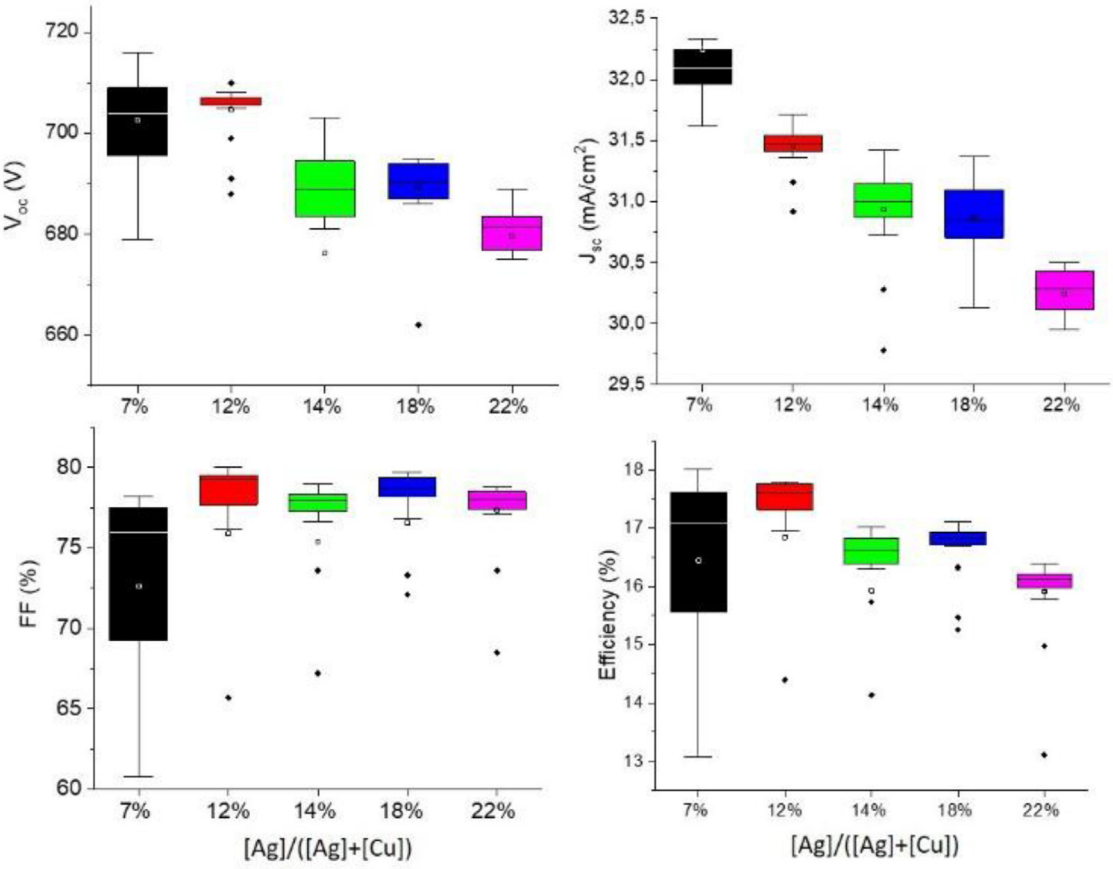

Fig. 1. Solar cell parameters as a function of the AAC ratio. Each box contains data from 20 cells.

2 Results and discussion

The current–voltage (J–V) parameters as a function of AAC ratio are shown in Figure 1. Each box contains data from 20 cells. A systematic decline in both the open-circuit voltage (V_{oc}) and the short-circuit current density (J_{sc}) is observed with increasing Ag. The FF shows an improvement from 7 to 12% AAC, and remains unaffected by AAC for higher Ag values. The best conversion efficiencies were obtained for the samples with lower Ag contents of 7% and 12%. The impact of Ag on the material and device properties leading to the observed solar cell parameters is analyzed below. Increased Ag content results in a flattened GGI profile of the absorbers as shown in the GDOES data in Figure 2a. A similar impact on GGI profile due to Ag incorporation in CIGS was observed by Yang et al. [4] and assigned to enhanced elemental diffusion [5]. The flattened GGI profile increases the minimum band gap of the absorber. This is visible in the internal quantum efficiency curves shown in Figure 2b. Substitution of Cu with Ag has been shown to affect the band gap of ACIGS absorber [6]. The predicted band-gap changes are significant for Ag contents higher than 40% or for GGI contents higher than 50%. Therefore, in the compositional range presented here, the observed systematic decrease in the J_{sc} with increasing Ag (Fig. 1) can be explained by the flattened GGI profile. The characteristic energies of Urbach tails extrapolated from the QE measurements based on a method described in reference [7] are shown in Table 1. The Urbach-energy values vary between 16.6 meV and 19.0 meV, but do not show a trend with increasing Ag content, in contrast to observations reported in the literature [4].

To calculate the impact of the grading profiles on the solar-cell parameters, and to separate it from the other properties affected by Ag incorporation, the measured GGI profiles were imported into a model created with SCAPS-1D software. The simulated change in V_{oc} only due to the change in GGI profile is shown in the inset in Figure 2a. The impact of the flattened GGI profile on the V_{oc} is twofold: on one side, the V_{oc} increases due to the band-gap increase near the absorber/buffer interface. The second effect of the flattened GGI profile is a decreased back grading, which lowers the back-contact barrier and allows more back-contact recombination. The increased back-contact recombination reduces the V_{oc}, therefore reducing the benefit of increased band gap at the notch. The result is a V_{oc} increase for low Ag contents followed by its saturation for higher Ag values. The V_{oc} increase due to the GGI profile is opposite to the experimentally observed trend that shows a decrease in V_{oc} with increasing Ag (see Fig. 1). This suggests an existence of a V_{oc} loss mechanism, which overwhelms the improvement due to the GGI profile. The radiative V_{oc} limit calculated based on the method described in references [7,8] is shown in Table 1, as well as the measured

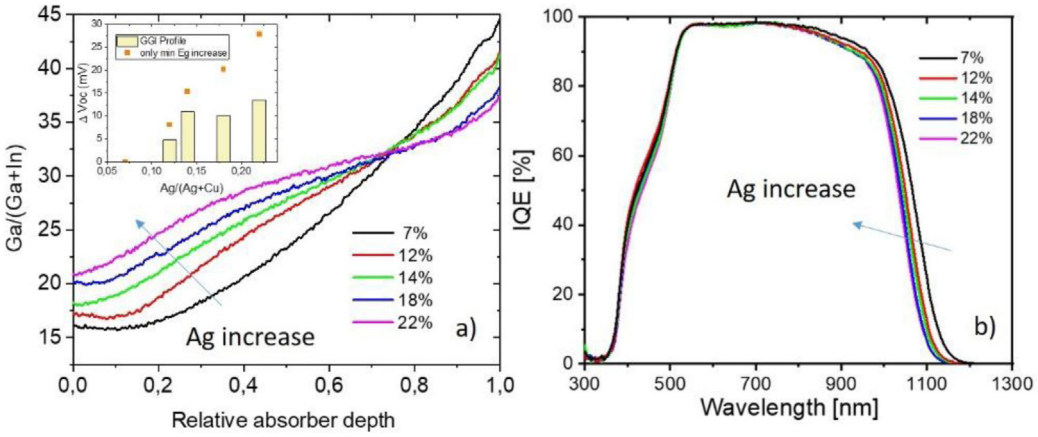

Fig. 2. (a) GGI profile measured by GDOES, inset: A simulated change in V_{oc} due of the changed Ga profile (bars) and a simulated change in V_{oc} due to increased band gap at the notch (squares). (b) Internal quantum efficiency curves of the cells with different Ag contents.

Table 1. Minimum absorber band gap energy determined from the IQE data, Urbach energy calculated from QE, radiative V_{oc} limit calculated from QE, measured V_{oc} of the best cells for each AAC and their difference, $\Delta V_{oc} = V_{oc}$ (radiative) $- V_{oc}$ (measured), representing nonradiative V_{oc} losses.

AAC (%)	E_g optical (eV)	Urbach energy (meV)	V_{oc} radiative (mV)	V_{oc} exp. (mV)	ΔV_{oc} (mV)
7	1.132	16.6	878	716	162
12	1.153	18.4	897	707	190
14	1.158	16.8	902	700	202
18	1.165	19.1	909	694	215
22	1.169	17.0	910	685	225

V_{oc} of the best cell for each Ag content. The difference between the two values shows that the non-radiative losses increase with the Ag content.

The apparent carrier densities derived from room-temperature capacitance–voltage measurements are shown in Figure 3a. Two cells from each Ag content are presented and they show similar carrier density values. Increased Ag results in a reduced hole density in CIGS.

Decreased carrier density due to Ag addition has also been reported in literature [9–11]. Our ToF-SIMS measurements shown in Figure 4a show that Na content increases with increased Ag.

An increase in Na concentration with an increased AAC was also reported in reference [12] and assigned to the Na-solubility in the grain interiors. In addition, the Rb content, with an exception of the 7% device, does not show a dependence on Ag (Fig. 4b). As Rb is generally found at the grain boundaries, the observed decrease in Rb content from 7% AAC to 12% AAC can be correlated to the strong increase of CIGS grain size (see the SEM image in Fig. 6).

To have a further look into the recombination mechanisms, current-voltage curves were measured at different temperatures and at different illumination intensities. The dependence of V_{oc} on temperature is shown in Figure 3b. The $V_{oc}(T)$ curves were fitted from 200 K to 290 K and extrapolated to $T = 0$ K. The 0 K intercepts are close to the band-gap values for the devices with 7%, 12% and 14% Ag. For the devices with 18% and 22% Ag, despite the band-gap increase, the $V_{oc}(T)$ curves interpolate at 0 K to a slightly lower value. The activation energy extracted from the $V_{oc}(T)$ for the 18%-Ag device is 13 meV lower than its band gap, and for the device with 22% Ag 26 meV below the band gap.

The combined results from the temperature-dependent JV curves, JV curves measured at different illumination intensities, and CV measurements were used for a recombination analysis suggested by the references [13,14]. The analysis was performed on ten cells (the best ones from each test substrate). The recombination coefficients at 0 V are shown in Table 2: in the depletion region, R_0^d, in the bulk R_0^b, and at the interface, R_0^i. The recombination coefficients at the interface and in the bulk (with a diode quality factor $n = 1$) show a systematic increase with Ag content. The depletion region recombination coefficient ($n = 2$), does not show a clear dependence on the Ag content.

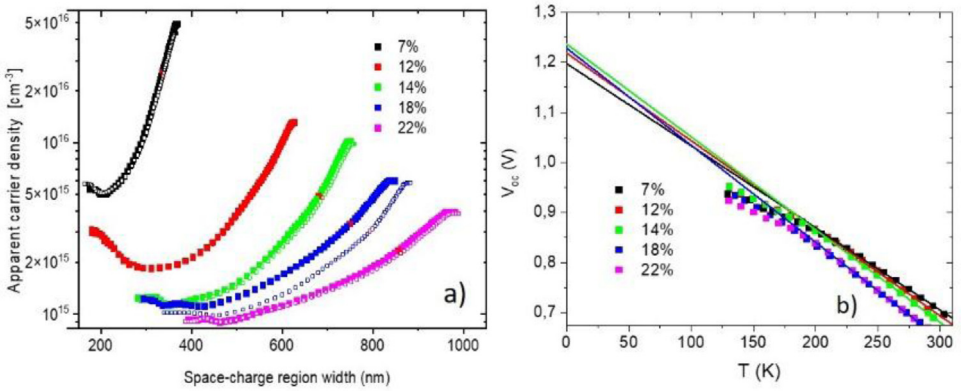

Fig. 3. (a) Apparent carrier density from capacitance-voltage data. Two cells representing each Ag content are shown. (b) V_{oc} as a function of temperature extrapolated to 0 K.

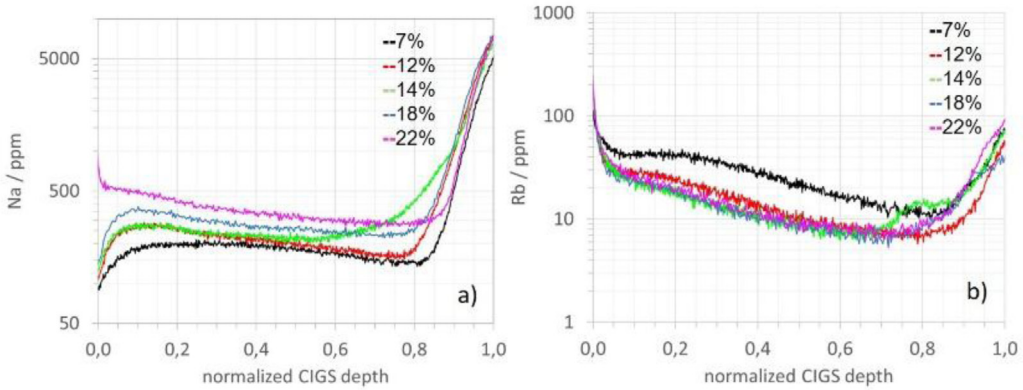

Fig. 4. ToF-SIMS measurement results showing the (a) Na and (b) Rb content for samples with different AAC.

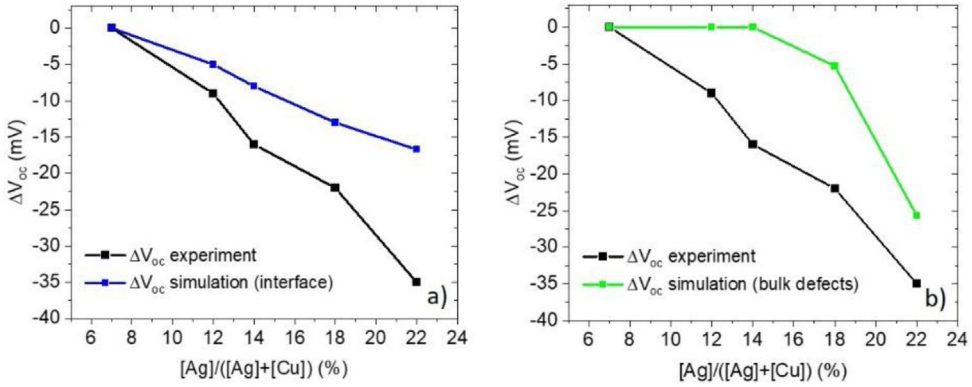

Fig. 5. Simulated change in V_{oc} as a result of interface- and bulk- recombination rate variation as predicted by the recombination coefficients in Table 2.

The changes in interface and bulk recombination were incorporated into a SCAPS model and their impact on the V_{oc} was calculated (Fig. 5). The increased recombination partially explains the observed V_{oc} losses with increasing Ag.

Increased AAC ratio results in a better crystalline quality, as seen in the SEM results in Figure 6. The devices with higher Ag contents have larger grains and a smoother surface.

3 Conclusions

In summary, an analysis of a series of CIGS devices with different AAC ratios showed that a partial substitution of Cu with Ag in the CIGS absorber affects multiple structural as well as electronic properties.

The Ag substitution flattens the GGI grading in the absorber, thus decreasing the J_{sc}. The V_{oc} systematically decreases with an increased Ag content due to a decreased

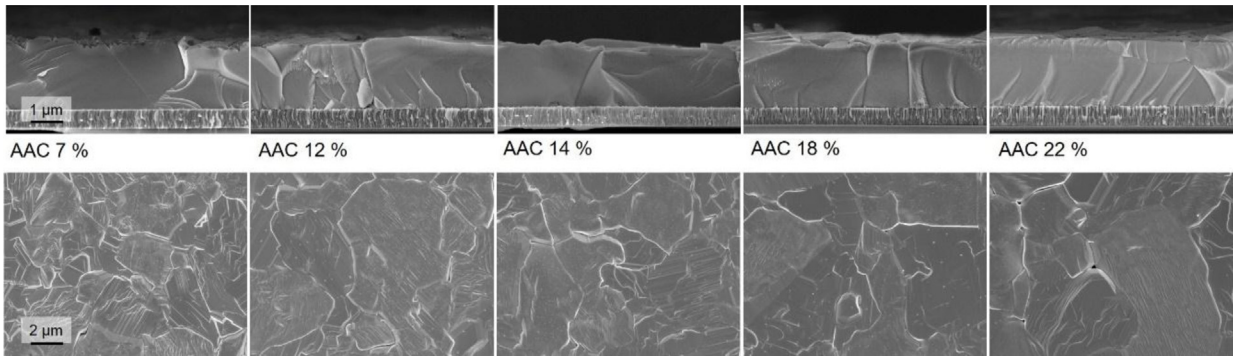

Fig. 6. Cross-sectional (above) and top view (below) SEM images of the samples for different AAC contents.

Table 2. Recombination coefficients in the devices with different Ag contents.

Ag/(Ag+Cu) (%)	R_0^d ($cm^{-2}s^{-1}$)	R_0^i ($cm^{-2}s^{-1}$)	R_0^b ($cm^{-2}s^{-1}$)	W (µm)
7	$4.32 \cdot 10^{11}$	$5.74 \cdot 10^{5}$	$1.90 \cdot 10^{5}$	0.306
12	$2.74 \cdot 10^{11}$	$1.06 \cdot 10^{6}$	$1.80 \cdot 10^{5}$	0.489
14	$6.69 \cdot 10^{11}$	$1.42 \cdot 10^{6}$	$1.75 \cdot 10^{5}$	0.598
18	$4.64 \cdot 10^{11}$	$2.23 \cdot 10^{6}$	$2.47 \cdot 10^{5}$	0.660
22	$6.76 \cdot 10^{11}$	$2.91 \cdot 10^{6}$	$4.59 \cdot 10^{5}$	0.744

carrier density as well as increased non-radiative recombination losses.

Despite the slight decline in the performance due to a decreased hole density and an increased recombination, the devices with higher Ag contents have advantages of a lower temperature growth and flatter surfaces.

This work was supported by the German Federal Ministry for Economic Affairs and Climate Action (BMWK) under the contracts numbered 03EE1078 (ODINCIGS) and 0324353A (CIGSTheoMax). The simulations were performed with a SCAPS-1D software developed at the University of Ghent, Belgium.

Author contribution statement

Ana Kanevce performed the device characterization, SCAPS simulations and the data analysis. Stephanie Essig, Stefan Paetel and Dimitrios Hariskos grew the samples studied. The material characterization, the ToF-SIMS measurements and the SEM measurements were done by Wolfram Hempel and Theresa Magorian Friedlmeier respectively. In addition, all of the authors contributed to the discussions and provided valuable insights.

References

1. L. Chen et al., IEEE J. Photovolt. **4**, 1 (2014)
2. S. Essig et al., J. Phys. Mater. **4**, 024003 (2021)
3. A. Kanevce et al., Eur. Phys. J. Photovoltaics **11**, 8 (2020)
4. S.C. Yang et al., Sol. RRL **5**, 2100108 (2021)
5. G. Kim et al., ACS Appl. Mater. Interfaces **11**, 31923 (2019)
6. J. Keller et al., Prog. Photovolt. Res. Appl. **28**, 237 (2020)
7. L. Krückemeier et al., Adv. Energy Mater. **10**, 1902573 (2020)
8. T. Kirchartz, U. Rau, J. Appl. Phys. **102**, 104510 (2007)
9. N. Valdes et al., Sol. Energy Mater. Sol. Cells **195**, 155 (2019)
10. R.L. Garris et al., Sol. Energy Mater. Sol. Cells **174**, 7783 (2018)
11. C.P. Thompson et al., in *Conf. Proc. IEEE Photovolt. Spec. Conf.* (2015), pp. 1-6
12. H. Aboulfadl et al., ACS Appl. Mater. Interfaces **13**, 71888 (2021)
13. J.V. Li et al., Sol. Energy Mater. Sol. Cells **124**, 143 (2014)
14. S. Grover et al., Appl. Phys. Lett. **103**, 093502 (2012)

Cite this article as: Ana Kanevce, Stephanie Essig, Stefan Paetel, Wolfram Hempel, Dimitrios Hariskos, Theresa Magorian Friedlmeier, Impact of Ag content on device properties of Cu(In,Ga)Se_2 solar cells, EPJ Photovoltaics **13**, 28 (2022)